ECLAT Deliverable 310.1: Description of 1D and 2D equivalent current data generation

Max van de Kamp, Liisa Juusola and Kirsti Kauristie

Finnish Meteorological Institute

August 2012

1 Introduction

1.1. ECLAT project

The European Cluster Assimilation Technology (ECLAT) project funded by the EU FP7 programme provides a selection of useful supporting data sets to the Cluster Active Archive [Laakso et al., 2009]. The Finnish Meteorological Institute conducts in ECLAT the work packages 310 and 320, in which ionospheric equivalent current vectors are computed in the Fennoscandia region where the MIRACLE network of magnetometers and auroral cameras are operated. The MIRACLE magnetometer network is often called (also in this text) as the IMAGE network, which should not be confused with the IMAGE satellite, whose data products are generated in ECLAT work package 430. The equivalent currents are provided as one-dimensional data (1D, eastward current intensities as function of time along the IMAGE network central longitude) and two-dimensional data (2D, current vectors in a latitude-longitude grid).

The equivalent current vector data are provided in the Cluster Exchange Format (CEF) (see Section 5.1). Also, quick-look plots are provided to facilitate event-selection from the massive data set (see Section 6.1).

1.2. Equivalent currents

Equivalent ionospheric currents are a convenient means to study the characteristics of the currents in the ionosphere. These currents are directly connected to the field-aligned magnetospheric currents, though ionosphere-magnetosphere coupling [e.g. Kamide and Baumjohann, 1993]. These magnetospheric currents are strongly dependent on solar activity, and the ionospheric currents reflect those solar-dependent magnetospheric current variations. Since strong disturbances in the ionospheric currents can affect technological systems on the ground [e.g. Boteler et al., 1998], there is a great interest in the dynamics of these currents in relation to solar activity.

The concept of 'equivalent' currents models the ionospheric currents as present in a thin shell, usually the highly conductive E-layer at 100 km height, and represent only the divergence-free part of the total currents. Still, under many circumstances they give valuable information about spatial and temporal characteristics of the real 3-D ionospheric currents [e.g. Untiedt and Baumjohann, 1993]. The short-term variations of these equivalent currents can effectively be estimated from magnetometer measurements from a two-dimensional ground magnetometer network.

In this project, equivalent currents are analysed for an area over Fennoscandinavia, over the period 2001-2010. For the equivalent current estimate, use is made of the method of spherical elementary current systems [Amm and Viljanen, 1999; Pulkkinen et al., 2003]. The calculations are described in more detail in Section 3. The source data used as input for this are described in the next subsection.

For the calculation of the equivalent currents, only the X- (north) and Y- (east) components of the magnetic field at all stations are necessary.

1.3. IMAGE Magnetometer measurements

The input data for the calculation of the ionospheric currents in the project ECLAT are the magnetometer returns of the Scandinavian ground magnetometer network IMAGE (http://space.fmi.fi/image/beta/). This network consists of 32 magnetometers over geographic latitudes from 58 to 79 degrees, which is especially favourable for electrojet studies. The magnetometers return data at a time resolution of 10 seconds.

Figure 1 shows a map of the locations of the magnetometers of the IMAGE Network. Table 1 lists their names and geographic coordinates. Figure 2 shows the availability of the IMAGE recordings since the days when the network was established.

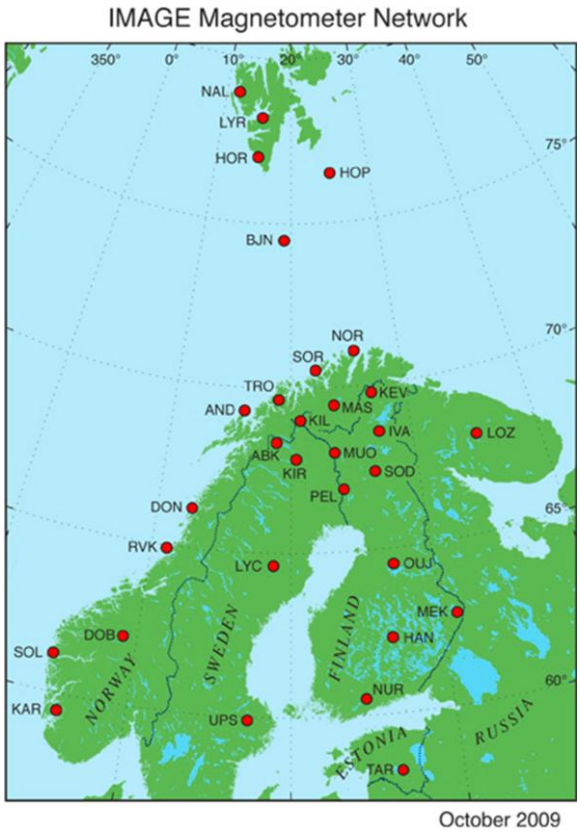

Figure 1. Map of the IMAGE magnetometer stations.

Table 1: Codes, names and locations of all IMAGE stations.

Station	Name	latitude (°)	longitude (°)
NAL	Ny Ålesund	78.92	11.95
LYR	Longyearbyen	78.20	15.82
HOR	Hornsund	77.00	15.60
HOP	Hopen Island	76.51	25.01
BJN	Bjørnøya	74.50	19.20
NOR	Nordkapp	71.09	25.79
SOR	Sørøya	70.54	22.22
KEV	Kevo	69.76	27.01
TRO	Tromsø	69.66	18.94
MAS	Masi	69.46	23.70
AND	Andenes	69.30	16.03
KIL	Kilpisjärvi	69.06	20.77
IVA	Ivalo	68.56	27.29
ABK	Abisko	68.35	18.82
LEK	Leknes	68.13	13.54
MUO	Muonio	68.02	23.53
LOZ	Lovozero	67.97	35.08
KIR	Kiruna	67.84	20.42
SOD	Sodankylä	67.37	26.63
PEL	Pello	66.90	24.08
DON	Dønna	66.11	12.50
RVK	Rørvik	64.94	10.98
LYC	Lycksele	64.61	18.75
OUJ	Oulujärvi	64.52	27.23
MEK	Mekrijärvi	62.77	30.97
HAN	Hankasalmi	62.25	26.60
DOB	Dombås	62.07	9.11
SOL	Solund	61.08	4.84
NUR	Nurmijärvi	60.50	24.65
UPS	Uppsala	59.90	17.35
KAR	Karmøy	59.21	5.24
TAR	Tartu	58.26	26.46

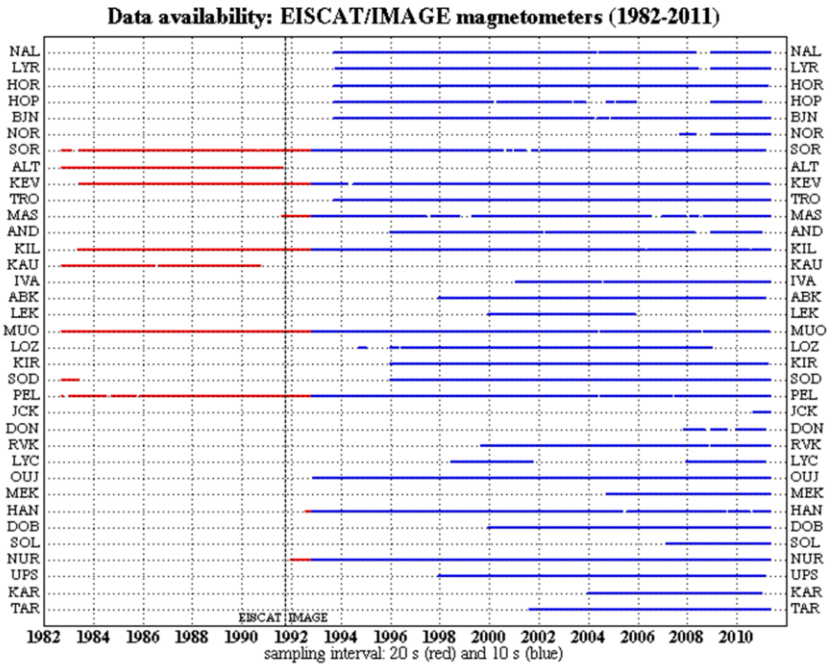

Figure 2. Availability of the IMAGE recordings .

1.4. Baselines

The measured magnetic field at the earth's surface is a superposition of the components originating from the inner earth and from electromagnetic effects caused by currents flowing the ionosphere and magnetosphere. As the internal magnetic field component is not interesting from the viewpoint of the ESA Cluster mission, it is usually subtracted from ground-based magnetic field measurements as "Solar quiet-variations (Sq variations)" before further analysis of the data. In addition, some magnetometer data contain system effects, which should also be subtracted before analysis. The Sq variations and the system effects are here treated together as "baselines".

In this project, a novel method for deriving the baselines of the magnetometer data has been developed. The method is suitable for processing extensive data sets and it is capable to handle also some of the most typical technical artefacts (jumps and instrument drifts) appearing occasionally in the recordings.

First in our approach, 'templates' are derived, based on the lowest few harmonics of the daily curves from the quietest days. The diurnal variation of the baseline is obtained by interpolating between these templates. This method ensures a smooth baseline at all times, avoiding any discontinuities at transitions between days or months. To obtain the full baseline, the diurnal variations are added to a long-term baseline which is obtained by interpolating between the daily median values. This way, the baseline is ensured to follow long-term trends, such as seasonal and tidal variations, as well as equipment drift.

The procedure for the baselines is described in detail in Section 2.

2 Baselines

2.1. Introduction

The traditional method of removing a baseline, or 'quiet day curve', from magnetometer data of a particular day, is to look for the magnetically quietest day in the same month as the day of interest, and assuming the magnetic field at this quiet day to be exclusively caused by long-term solar wind variations and diurnal variations in electron density in the ionosphere. This 'quiet day curve' is then subtracted from the curve for the day of interest, leaving only the effects caused by Coronal Mass Ejections and other disturbances. This method has several problems:

1. There may not be any day in the entire month which is completely free from disturbances. In this case, the 'quietest' day is not really 'quiet' and the baseline will still contain some disturbance effects.
2. The magnetometer data from any day, including the quiet ones, contain small fast random fluctuations. When these are subtracted from data of another day, the resulting rms of these fluctuations increases.
3. The data from the quiet day is in general at the end of the day not the same as that at the start of the day. Hence, if the baseline subtraction is performed for a period around midnight (e.g. to calculate equivalent ionospheric currents), a discontinuity will occur at midnight.
4. The quiet day curve will be different from month to month. This means that at midnight between the last day of a month and the first day of the next, the discontinuity may be even larger.
5. The magnetometer data generally contain slow variations over the course of several days, and longer (see the Section 2.2 for examples). As a consequence, the average value of the quiet day may not be representative for that of other days in the same month, which are up to 30 days earlier or later.

In literature e.g. Janzhura and Troshichev [2008] and Stauning [2011] have presented methods for baseline derivation which overcome most of the above listed problems. These methods, however, are not suitable for the task of WP 310, since they are difficult to use in massive data processing. In this paper, a method is described which overcomes all the above problems, and in addition is simpler than the method by Janzhura and Troshichev. The procedure will be described in the following sections.

2.2. Long-term baseline

To determine the baseline, first the part is considered which consists of the long-term variations in the magnetic field, i.e. variations over periods longer than 24 hours, i.e. on the scale of days, months, or years. These variations will be represented in the baseline by determining from every day of data a single daily 'background' value (for each station and for each field component). For this value it might be considered to use the average of the measured data, however, rather than this, the median is considered more stable, as being less sensitive to extreme values during disturbed days.

The median value is calculated for every day of data. The long-term baseline is considered to be equal to the median for 12:00 UT at the respective day. At any other time, the long-term baseline is interpolated between these values. The long-term baseline will be referred to in this paper as Q_L. This quantity is time-dependent and station-dependent, and is defined separately for the different field components.

Figure 3 shows this daily median calculated over various periods of data, and demonstrates the long-term variations revealed by it. This graph shows that these variations consist of, among others, the following components:

Secular variations: due to very slow variations in the earth's internal magnetic field pattern, the *y*- and *z*- components of the magnetic field at all IMAGE stations steadily increased, at a rate of slightly over 35 nT/year, during the period 2001-2010. (The *x*-component did not change significantly.) The upper left-hand graph of Figure 3 demonstrates this for B_y in Uppsala.

Seasonal variations: The seasonal changes in the ionospheric conductance and in the ionosphere-thermosphere-magnetosphere interactions result in variations in all magnetic field components with a period length of one year. As an example, the upper right-hand graph of Figure 3 shows that B_x in Uppsala oscillated at about 10 nT peak-to-peak within the years of 2008 and 2009.

Tidal variations: variations with periods in the order of about one month can be observed, which are likely the result of changes in the global distribution of the ionosphere due to lunar attraction, which have an effect on the magnetic field measured on the ground. As an example, the lower left-hand graph of Figure 3 shows that B_x in Uppsala varied at this frequency at about 15 nT peak-to-peak in October to December 2007.

Equipment drift: some of the magnetometers occasionally exhibited some variations over the course of one or a few days, which did not repeat, and showed no correlation with space weather parameters or with any of the other magnetometer results. The lower right-hand graph shows an example for Sørøya, where on 23 December 2009, the readings for B_x sank by 80 nT over two days, and then gradually recovered, over the course of 18 days.

The equipment drifts especially happened at the stations in remote locations, which are not continuously manned and monitored. These drifts should obviously be classified as measurement errors. However, if they can be quantified using the current method, they can be removed along with the above-mentioned long-term variations in the magnetic field, which means that these low-quality data do not need to be discarded. This is a very useful outcome, since these magnetometer stations in remote places often are some of the most crucial ones. Many of them are located in northern Scandinavia and the sea between Norway and Svalbard, which is an area where much of the magnetic activity occurs, but not many magnetometers are present, due to the difficult accessibility of the area. This is why magnetometers were placed in this locations in the first place, despite their inaccessibility. It is therefore very useful if these relatively valuable results, even if not of perfect quality, can still be used in ionospheric analyses.

Obviously, during magnetically very disturbed periods, the median value calculated over a day may not be representative for the long-term baseline. In these cases, the median of these particular disturbed days will not be used, but the long-term baseline will be interpolated between other

median values. Further on, it will be shown how the classification of these 'usable' median values is performed.

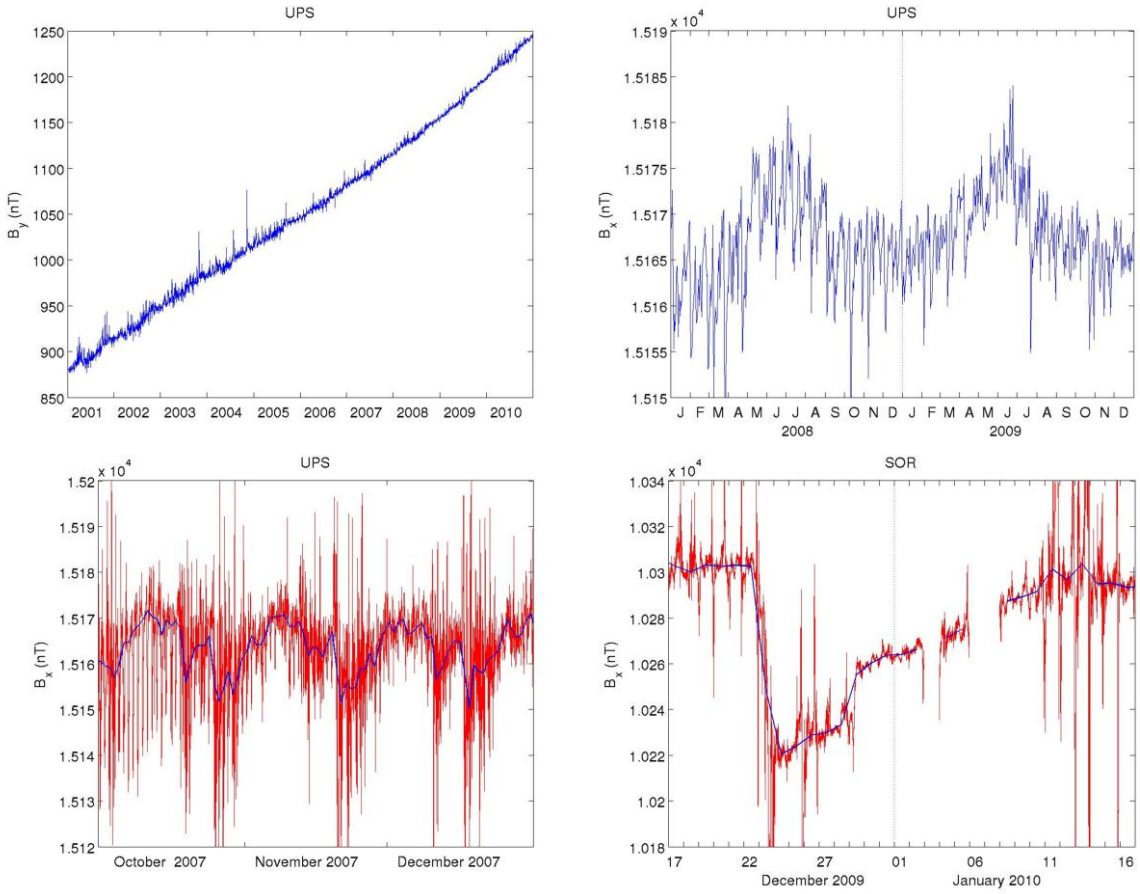

Figure 3. Daily median values of magnetometer data (blue), demonstrating the long-term variations.

- *Top left: secular variation in B_y in Uppsala over the full 10-year period;*
- *Top right: seasonal variations in B_x in Uppsala over 2008-2009;*
- *Bottom left: tidal effects in B_x in Uppsala in autumn 2007 (raw data included in red);*
- *Bottom right: equipment drift in B_x in Sørøya in December 2009 (raw data in red).*

2.3. Quiet days

For every separate magnetometer station, a list of the quietest days of each month is generated.

At any magnetometer station, a day is considered 'quiet' if the magnetic field variations measured on this day are as much as possible caused by Sq variations and not by magnetic disturbances. Hence, a 'quiet' day would mainly contain slow variations; its fast variations should be relatively small compared to the slow variations.

Because the fast variations due to disturbances are mostly much larger than the Sq variations, it seems logical to calculate simply the standard deviation of every day of data, and look for the smallest standard deviations of each month. Indeed this method works reasonably, however there are cases where this method is too coarse, as will be shown below.

In the method of this paper, the quiet day selection is performed as follows. Each day of data is partitioned into 24 one-hour sections. In each one-hour section, a straight line is fitted to the data, for the x- and y- components of the magnetic field. This straight line is subtracted from the data, and from the remaining data, the hourly standard deviation, σ_H, is calculated. The result of this is 2x24 values (2 components and 24 hours) of σ_H per day per station. Of these 48 values, the daily maximum is calculated, referred to as σ_{Hmax}. These values of σ_{Hmax} are the indicators for days with or without disturbances: of each month, the day with the lowest σ_{Hmax} is selected as the 'quiet day' for that month, at that station.

As an extra requirement, the 'quiet day' should contain no data gaps, so only days with 100% data availability for all magnetic components can be potential candidates for any month's 'quiet day'.

Figure 4 demonstrates this procedure, showing B_x in Oulujärvi on three different days in March 2002. The day shown in the bottom two graphs, March 28, resulted from this procedure as the quietest day of this month (note that this procedure also takes into account the *y*-component of the magnetic field, which is not shown in the figure).

This procedure works better than calculating the overall standard deviation of the whole day, because a day with a very smooth curve consisting of only Sq variations may have a larger standard deviation than a day with some disturbances.

Of course, even though according to this procedure a 'quietest' day of each month can always be found (as long as at least one full day of data is available), it may be that this quietest day still contains too much magnetic disturbance to be used for a quiet day curve. Especially during and around the solar active year of 2003, disturbances can be so frequent, that not necessarily a full day can be found within every month where these disturbances are insignificantly small. In other words: the 'quietest' day of the month may not be really 'quiet'.

Because of this, an extra criterion is applied: if for any month, the value of σ_{Hmax} of the quiet day is above a certain threshold value, then this quiet day is discarded and no quiet day is assigned for this month. Later it will be shown how these cases are dealt with in the rest of the procedure. The optimum threshold value of σ_{Hmax} to be used for this, depends on the typical level of both slow and fast variations in the magnetic field, and therefore varies from station to station. The values used were optimised empirically; the results are listed for all IMAGE station in Table 2. Using these threshold values, generally no more than three consecutive months without quiet days were encountered for any station in the entire IMAGE database 2001-2010.

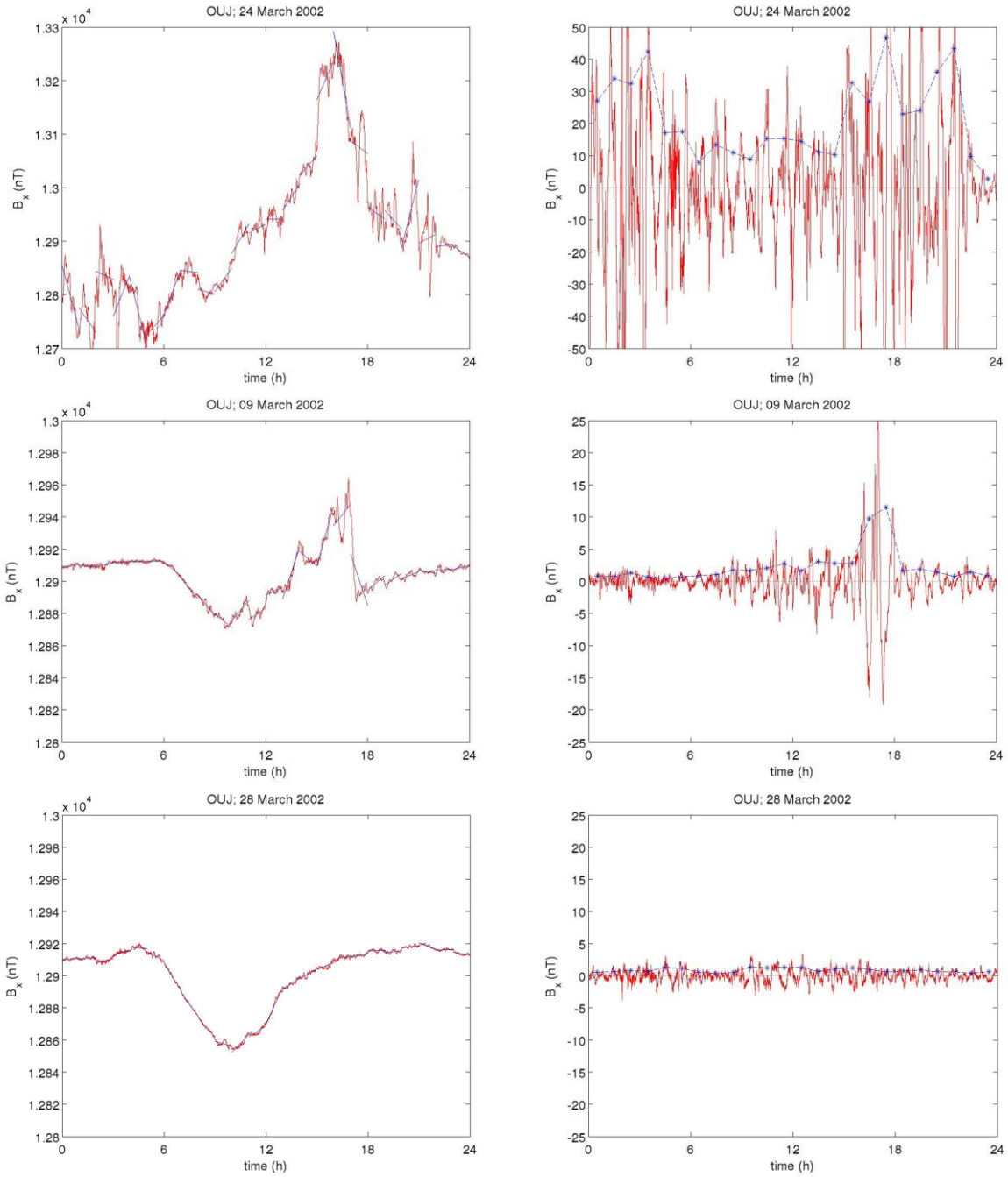

Figure 4. The quiet day selection procedure, demonstrated by the B_x-field in Oulujärvi in March 2002. Left-hand graphs: raw data and the hourly fitted lines fitted to it. Right-hand graphs: the data after subtraction of the fitted lines, and the calculated hourly standard deviations. Top: on a disturbed day; center: on a mostly quiet day with some disturbance; bottom: on a quiet day. The maximum σ_H values (from B_x alone) are: 46.7 nT, 11.5 nT, and 1.4 nT respectively.

2.4. Very disturbed days

The information of the hourly standard deviations σ_H, calculated as described in the previous section, will also be used to classify certain days as too disturbed to calculate the median value from, which would be used for determination of the long-term baseline Q_L (see Section 2.2).

In the top graph of Figure 5, three days of B_x-data from Abisko in November 2001 are shown, along with their daily median values. On November 4, conditions are mostly quiet, and the median value is a good representative of the long-term baseline. On November 5, some disturbances start late in the day, but the median value is not significantly affected by it. However, on November 6, conditions are disturbed all day, and the median value is dominated by these disturbances, and unsuitable to be used for the long-term baseline.

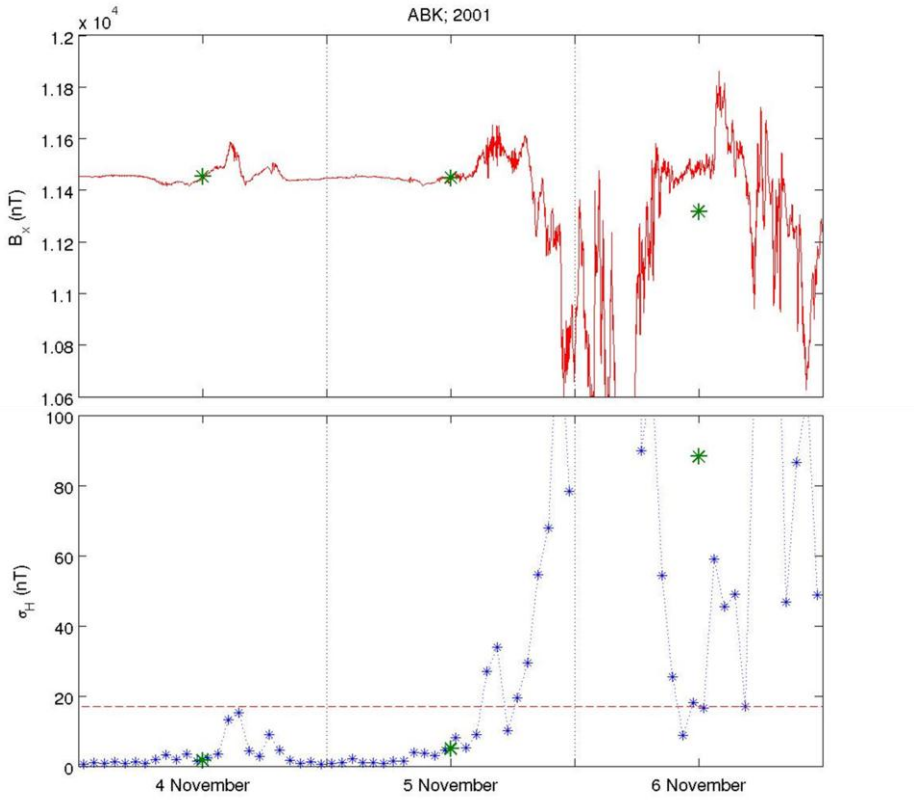

Figure 5. Top graph: B_x in Abisko on 4-6 November 2001, and the daily median values calculated from it (green stars). Bottom graph: hourly standard deviations σ_H of these data (blue stars), daily medians σ_{Hmed} of these (green stars),and suggested threshold value for σ_{Hmed} of Bx in Abisko (red).

Generally, a median value is relatively insensitive to irregularities in data as long as these irregularities consist of less than half of the data. Because of this, it is assumed that the daily median value will be unreliable, if (and only if) more than half of the day's hourly standard deviations σ_H indicate disturbed data during their hours (as in the previous section). These cases are clearly illustrated in the bottom graph of Figure 5, where the σ_H values of the data in the upper graph are shown.

This criterion is easily represented by the median value of the day's hourly standard deviation: σ_{Hmed}. If σ_{Hmed} is above a certain threshold, this means that at least half the σ_H values are above this threshold. This can be seen in the bottom graph of Figure 5, where σ_{Hmed} are the green '*' signs. As a threshold value of B_x for Abisko, 17 nT was empirically chosen (dashed line in Figure 5).

The decision whether a median value is used for the long-term baseline Q_L is made separately for B_x and B_y. Because typical variations in B_y are often different from those in B_x, also different threshold

values for these two are used. Furthermore, the threshold values are dependent on station location, just as is the case for the threshold of σ_{Hmax} (see previous section). All different threshold values were empirically adjusted; their values are included in Table 2.

Figure 6 shows an example of the result of this procedure, by the B_x-field in Oulujärvi in April 2010. These data contain some long-term baseline development, as well as some irregularities. Using the procedure described in this section, the median values of the entire month except April 5-7 were considered suitable for the long-term baseline. The long-term baseline Q_L, interpolated between the suitable median values, follows the long-term behaviour well, and is unaffected by the disturbance on April 5-7.

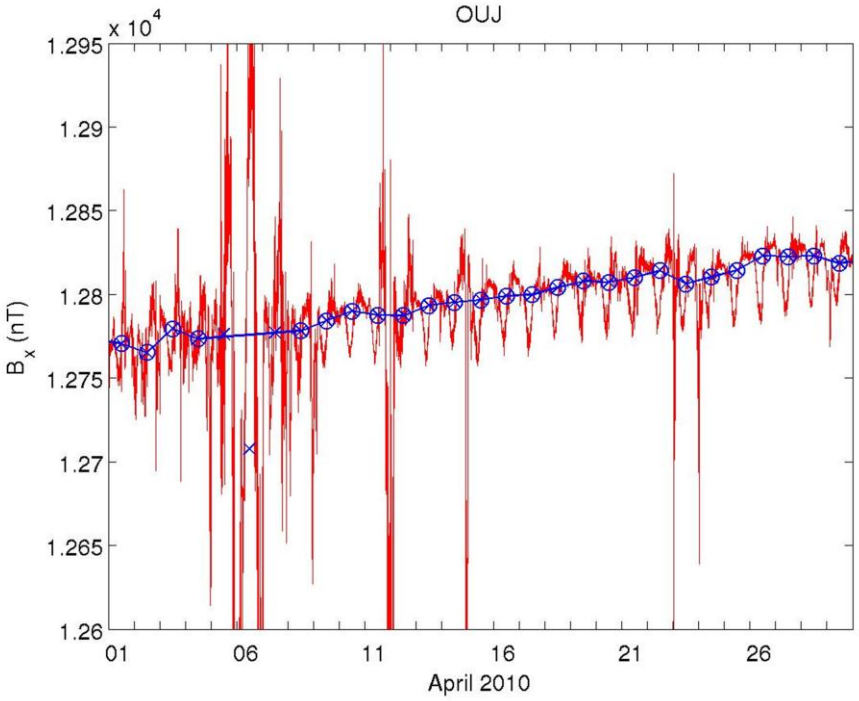

Figure 6. B_x-field in Oulujärvi in April 2010 (red), the daily median values (blue x), the ones of these that are qualified to be used for the long-term baseline (circles), and this baseline Q_L (blue solid line).

Table 2: Threshold values of σ_{Hmax} and σ_{Hmed} for each IMAGE station.

Station	Name	latitude (°)	longitude (°)	Threshold σ_{Hmax} (nT)	Threshold $\sigma_{Hmed,}$ B_x (nT)	Threshold $\sigma_{Hmed,}$ B_y (nT)
NAL	Ny Ålesund	78.92	11.95	18	14	13
LYR	Longyearbyen	78.20	15.82	21	16	15
HOR	Hornsund	77.00	15.60	25	20	17
HOP	Hopen Island	76.51	25.01	29	22	14
BJN	Bjørnøya	74.50	19.20	28	21	15
NOR	Nordkapp	71.09	25.79	19	25	12
SOR	Sørøya	70.54	22.22	20	20	12
KEV	Kevo	69.76	27.01	14	18	9
TRO	Tromsø	69.66	18.94	17	20	11
MAS	Masi	69.46	23.70	13	18	11
AND	Andenes	69.30	16.03	17	20	11
KIL	Kilpisjärvi	69.06	20.77	13	18	10
IVA	Ivalo	68.56	27.29	10	16	8
ABK	Abisko	68.35	18.82	11	17	10
LEK	Leknes	68.13	13.54	10	15	9
MUO	Muonio	68.02	23.53	9	15	8
LOZ	Lovozero	67.97	35.08	8	12	6
KIR	Kiruna	67.84	20.42	9	14	8
SOD	Sodankylä	67.37	26.63	8	13	7
PEL	Pello	66.90	24.08	7	12	7
DON	Dønna	66.11	12.50	7	11	6
RVK	Rørvik	64.94	10.98	6	9	5
LYC	Lycksele	64.61	18.75	8	19	7
OUJ	Oulujärvi	64.52	27.23	6	7	5
MEK	Mekrijärvi	62.77	30.97	5	4	4
HAN	Hankasalmi	62.25	26.60	5	4	4
DOB	Dombås	62.07	9.11	4	5	4
SOL	Solund	61.08	4.84	4	4	4
NUR	Nurmijärvi	60.50	24.65	4	5	3
UPS	Uppsala	59.90	17.35	4	4	3
KAR	Karmøy	59.21	5.24	4	3	3
TAR	Tartu	58.26	26.46	4	3	3

2.5. Templates composed of harmonics

Coming back to the subject of quiet days, defined in Section 2.3, this section describes how the diurnal variations are derived from these quiet days.

For every of the quiet days, the long-term baseline Q_L is subtracted from the data of the entire day. On the residual data, a Fast Fourier Transform (FFT) is performed. From the result of this, only the lowest few frequency components are retained. The number of frequency components can be chosen freely; in this paper it is suggested to use up to the 6th component. This means that only the first 7 (the 0th through the 6th) values resulting from the FFT are used. These complex values represent the amplitudes and phases of harmonics of frequencies which are all multiples of the inverse of 1 day. The frequencies of the first 7 harmonics are given in Table 3.

Table 3: Frequencies of the 7 lowest harmonics of data of 1 day.

harmonic nr.	*f* (Hz)	period
0	0	inf
1	1.1574 x10^{-5}	1 day
2	2.3148 x10^{-5}	12 h
3	3.4722 x10^{-5}	8 h
4	4.6296 x10^{-5}	6 h
5	5.7870 x10^{-5}	4h 48m
6	6.9444 x10^{-5}	4 h

The curve, composed of these 7 lowest harmonics of the quiet day, is equivalent to a low-pass filtered version of the quiet-day data. The resulting curve, which will here be called a 'template', will be used as a basis of the baseline construction. The template is described as follows:

$$T(t_d) = \sum_{h=0}^{6} |X_h| \cos\left(\frac{2\pi h t_d}{86400} + arg(X_h)\right) \quad (1)$$

where

t_d = 'time of day'; time elapsed since midnight (s)
h = index number of harmonic (0..6)
X_h = (complex) coefficient of harmonic h (nT)

There will be one set of harmonic coefficients X_h, and therefore one template $T(t)$, defined for each quiet day. One example day of data, and the template derived from it, are shown in Figure 7. Note that, for ease of comparison, Q_L has been subtracted from the data.

It's worth noting that since all the cosine arguments in equation (1) cover an exact number of cycles over the length of one day (86400 s), the template value at midnight at the end of the day, i.e. T(86400 s), will always be equal to that at midnight at the start, T(0 s), thus ensuring continuity at midnight if the template would be used on consecutive days. However, the templates are not used directly as such for the baselines, which will be shown in the next subsection.

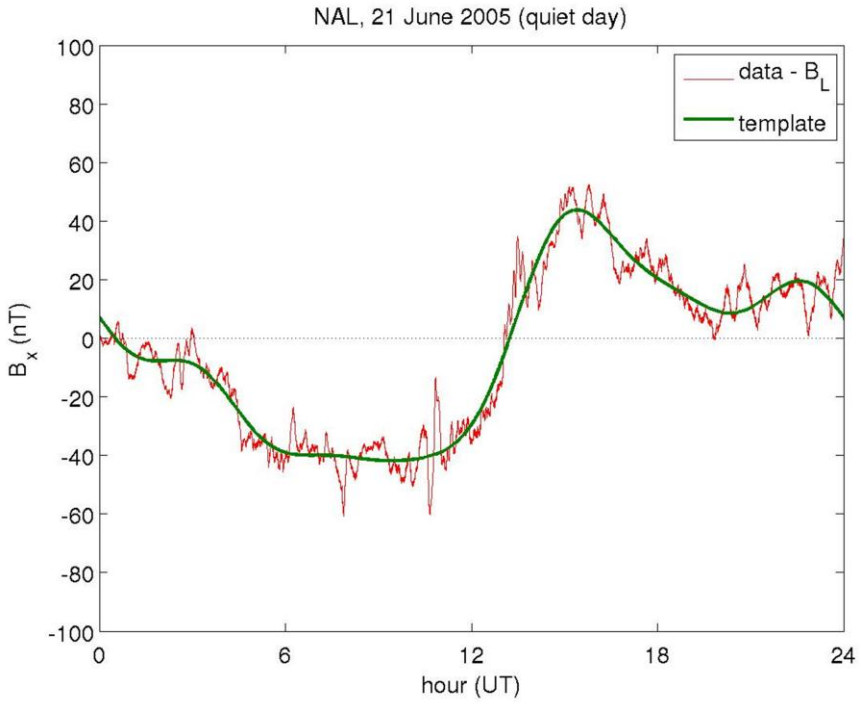

Figure 7. Red: B_x-field measured by the magnetometer in Ny-Ålesund (NAL) on 21 June 2005, one of the assigned quiet days, with the long-term baseline subtracted, leaving only the diurnal variation. Green: the template derived from this quiet day.

2.6. Diurnal baseline

As a next step, a curve representing the diurnal variation of background magnetic field is derived from the templates. This curve will be referred to as the 'diurnal baseline', and will be expressed as Q_D.

To obtain the diurnal baseline, the templates are interpolated continuously between midday on the previous assigned quiet day and midday on the next assigned quiet day. This can be expressed as follows:

$$Q_D(t) = T_1(t_d) + T_2(t_d) - T_1(t_d)\frac{t-t_1}{t_2-t_1} \quad (2)$$

where

t = the time point of interest (s)
t_d = 'time of day' as in equation (1), i.e. the remainder of t after division by 86400 (s)
$T_{1,2}$ = the template as a function of time of day on the previous resp. next quiet day
$t_{1,2}$ = the time point of midday on the previous resp. next quiet day (s)

It should be noted that, for the sake of consistency, also on the quiet days themselves the templates are interpolated. Consequently, only at noon, the diurnal baseline of a quiet day is exactly equal to the template of the same day. After noon, it is interpolated between this template and the next template, and before noon, it is interpolated with the previous template.

Figure 8 shows a schematic example, using imaginary templates consisting of only 1st harmonics. The blue curve is the template derived from quiet day 1 (on the left); the green curve is the template from quiet day 2 (on the right). The diurnal baseline (red curve) is interpolated between these two from midday on the first quiet day, to midday on the second quiet day. Only at noon on the quiet days (marked as 'o' in the graph), the baseline is equal to a template.

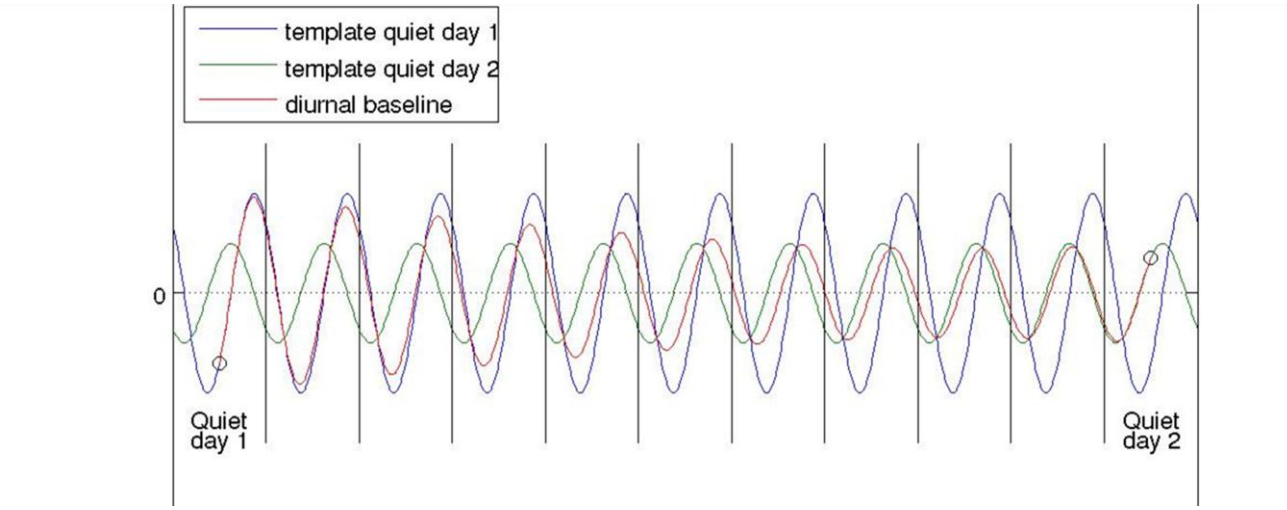

Figure 8. The principle of interpolation between templates. Templates derived from two consecutive quiet days, and the diurnal baseline, interpolated between them. The vertical lines mark midnights (separation between days).

2.7. Full baseline

To obtain the full baseline, the diurnal baseline Q_D is added to the long-term baseline Q_L :

$$Q(t) = Q_D(t) + Q_L(t) \tag{3}$$

where
Q = full baseline;
Q_D = diurnal baseline, derived from quiet days as described in Sections 2.3, 2.5 and 2.6;
Q_L = long-term baseline, derived from suitable median values as described in Sections 2.2 and 2.4.

Figure 9 presents an example of the result of the procedure described in this section. It shows the B_x-field in Uppsala from March 22 to April 10 in 2005 (two quiet days), and the corresponding baseline. In this example, the diurnal variation of the baseline follows that of the data not only on the assigned quiet days, but also on relatively quiet intervals in the middle of this period (e.g. April 1). Furthermore, the long-term (mostly tidal) variation of the data is well followed by the baseline.

The baselines derived as described in this section are produced for all IMAGE stations, over the 10-year period, with a 10-s time resolution (the same time resolution as the IMAGE data). The results are stored in files.

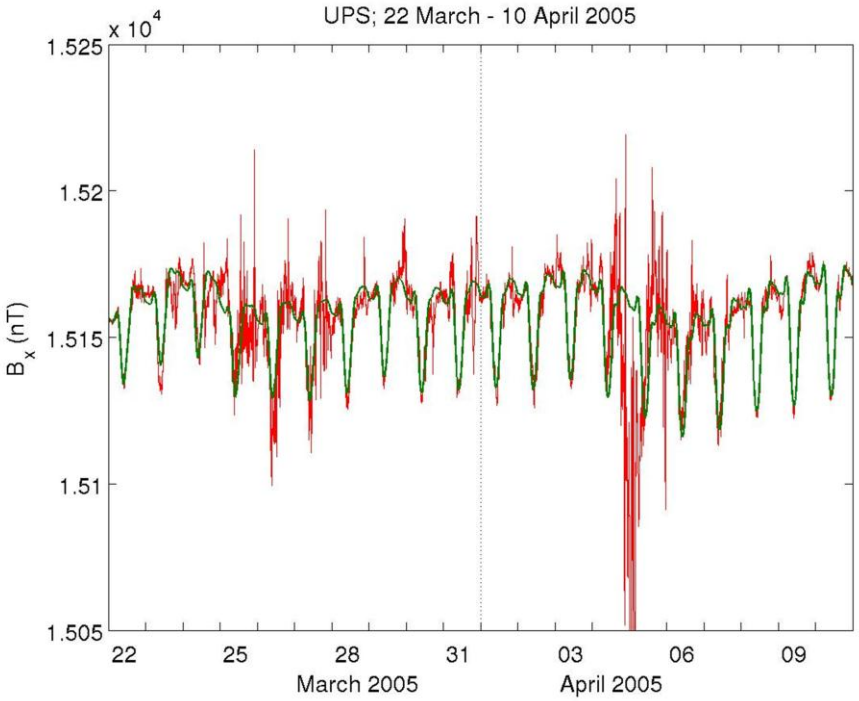

Figure 9. B_x-field at Uppsala from 22 March to 10 April 2005, and the corresponding baseline derived as described in this paper.

2.8. Baseline quality flag

Figure 10 shows an example for the B_x-field in December 2009 in Sørøya, which experienced some significant equipment drift in this period (also shown in Figure 3). The figure shows that the baseline derived for this period follows the equipment drift well, making this data reasonably usable for equivalent current calculations. Nevertheless, the data after removal of this baseline are probably still less accurate than those from a station without any equipment drift. Because of this, cases like this are labelled with a 'baseline quality flag', indicating a slightly doubtful condition from this station on these days.

Other cases which are labelled with a baseline quality flag, are days which are more than three months away from the nearest quiet day of the same station.

The baseline quality flag is included in the baseline output files, as a function of time, for each separate station. This information will be used in determining the full quality flag of the equivalent current result (see Section 4.2.4).

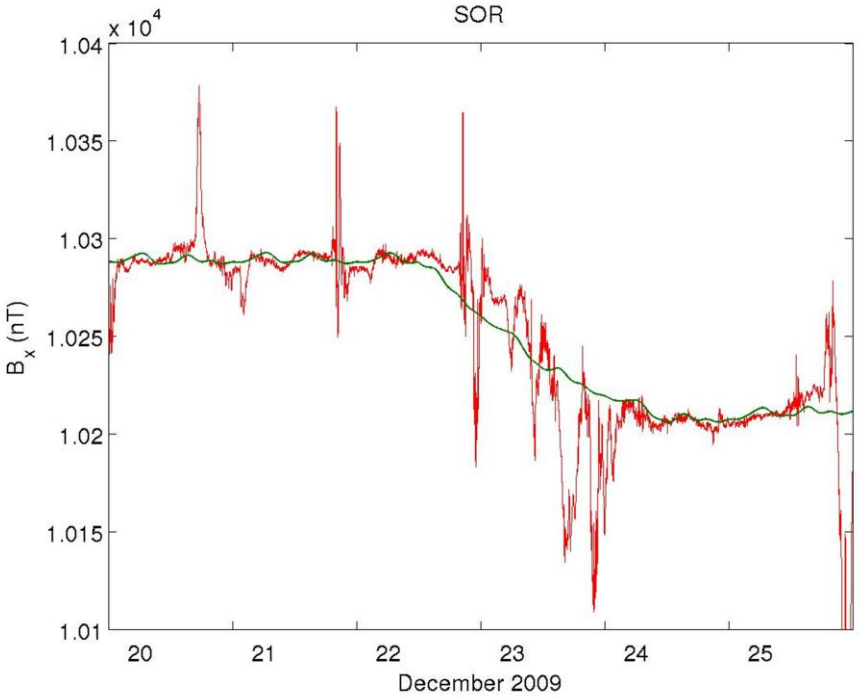

Figure 10. B_x-field at Sørøya from 20 to 25 December 2009, and the corresponding baseline derived as described in this paper.

3 Equivalent current computation

Once the baseline curves for each of the magnetometer stations have been determined, the actual equivalent current vectors are determined using the method of Spherical Elementary Current Systems (SECS) [Amm and Viljanen, 1999; Pulkkinen et al., 2003]. This method is based on the fact that the horizontal ionospheric currents, like any vector field on spherical surface, can be divided into divergence-free (df) and curl-free (cf) components. According to the current continuity equation in the ionosphere, the cf-component of horizontal currents close the field-aligned currents linking the upper atmosphere with magnetospheric processes.

The SECS technique can be used to solve the df-, cf, and field-aligned components of ionospheric currents from magnetic field vector measurements. Like shown by Fukushima [1976], the combined system of field-aligned currents and cf-component of horizontal currents cannot be observed from the ground surface. Therefore, from ground-based magnetometer data only the df-component (i.e. equivalent current) can be resolved. In WP310 this partial SECS-approach is used. If no steep gradients in the ionospheric conductances are present, equivalent currents roughly describe the distribution of ionospheric Hall currents.

In the SECS approach, the horizontal current density is expressed as a superposition of df- and cf elementary current systems (see Figure 11). In addition, radial field-aligned currents are added to the system so that they cover the divergence of cf-currents. The locations of the SECS-poles are distributed over the region of interest and each SECS is allowed to have a different amplitude. The magnetic fields caused by SECS can be expressed analytically which makes it possible to determine the SECS amplitudes by optimally matching the measured magnetic field with the superposed field generated by SECS.

SECS is a handy tool for analysis of ground-based magnetometer data as the locations of the SECS poles can be chosen freely to best accommodate the locations and density of the available measurement points. Thus different spatial resolutions can be achieved in different parts of the analysis region. It is good to remember, though, that magnetic variations caused by current systems with scale sizes less than 50 km attenuate strongly before they reach the earth surface. Therefore, ground-based magnetic field data are suitable for resolving of current systems with scale sizes larger than 50 km.

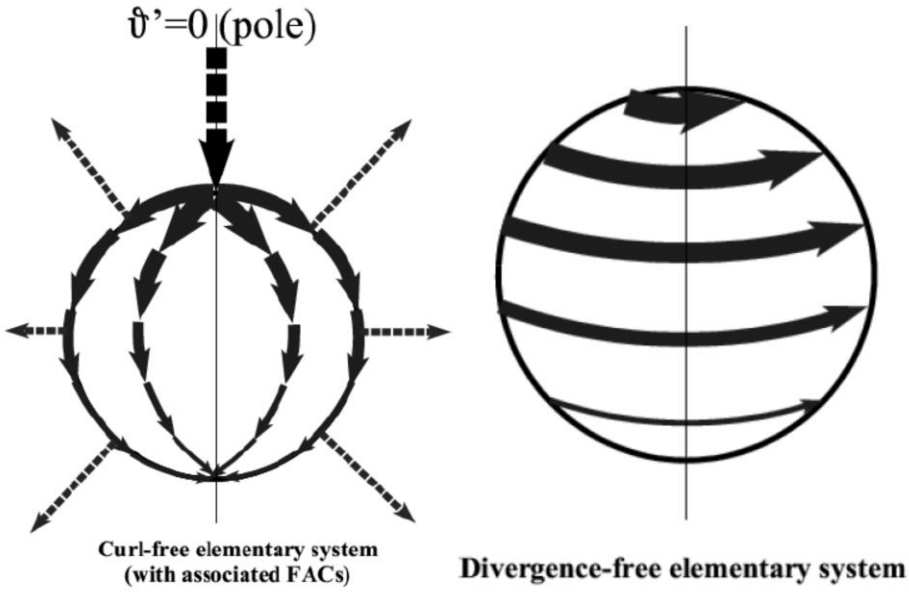

Figure 11. (Left) the curl-free elementary current system with the associated radial field-aligned currents and (Right) the divergence-free elementary current. Illustration by Olaf Amm.

4 Software modules

In this project, equivalent currents are analysed over the period 2001-2010. The software models used for this are described qualitatively in the following sections. The scripts have been written in MatLab language.

4.1. ECLAT_harmonicbaseline_2.m

This function determines the magnetometer baseline for one magnetometer station for a specified period of time.

4.1.1 Input variables

- The date&time (UT) at which the baseline is required. It is advisable to make this parameter equal to the time signature of the magnetometer data, from which this baseline is to be subtracted.
- A specification of the magnetometer station (see Table 1) for which the baseline is to be obtained.
- The number of harmonics to be used in the baseline derivation (not counting the 0th one). The highest harmonic used has a period length of 1 day divided by this number. (This input parameter is optional; if it is not given, the default of 6 harmonics will be used.)

4.1.2 Output variables

The output of the function consists of:

- The X-, Y-, and Z- component of the baseline of the magnetic field for the respective station.
- A summary of all information which is used in the derivation of this particular baseline. This consists of quiet-day dates, harmonic coefficients and median values (see Section 2 for explanations of these), 'jumps' in the data, and the baseline flag (see Section 2.8).

4.2. ECLAT_B2EQC.m

This module calculates, from a set of magnetometer measurements, the equivalent currents for a specified area. In the estimate, the currents are assumed to be in the E-layer at an altitude of 100 km above the earth's surface. The equivalent current is calculated for a horizontal spatial grid of: latitudes from 59.019° to 79.419° with a step size of 0.6°; and longitudes from 3.161° to 42.361° with a step size of 1.4°. The SECS poles used in the calculation are located at a grid of latitudes from 53.919° to 83.919° with a step size of 0.6°; and longitudes from 2.4607° to 43.0607° with a step size of 1.4°.

The software also produces a quality flag of the data, based on the availability of the magnetometer stations, the quality of the input data, and the estimated accuracy of the calculation in the specific configuration.

The software can handle any length of input data time series. In this project it is applied to magnetometer data files of exactly one day (UT) each time, i.e. 3652 separate files of the period 2001-2010.

4.2.1 Input variables

- The array of latitudes of the grid for which the equivalent currents are to be calculated.
- The array of longitudes of the grid for which the equivalent currents are to be calculated.
- The name(s) of the file(s) which hold(s) the input magnetometer data.

4.2.2 Input files

The script reads one or more file(s) of input magnetometer data. The file contains the following variables:

- the *X*- and *Y*-components of the measured magnetic field, with baselines subtracted and all possible errors removed.
- the latitudes, longitudes and name codes (Table 1) of the magnetometer stations.
- the date and time for each data point of magnetic field data.
- The baseline quality flag of all magnetometer stations (see Section 2.8).

4.2.3 Output files

The script produces an output file, containing the following variables:

- The radius of the earth used (km)
- The altitude above the earth's surface of the ionosphere assumed (km)
- The latitude and longitudes of the grid points (degrees)

  and for every time point (every data sample):

  - The year, month, day, hour, minute and second of the sample
  - The quality flag of the sample (see next subsection)
  - the northward component of the equivalent current (A/km) for every latitude and longitude.
  - the eastward component of the equivalent current (A/km) for every latitude and longitude.

4.2.4 Quality flag

The meaning of the quality flag is as follows:

1 The equivalent currents are in absolute value smaller than 50 mA/km over the entire area, which is too low to be a significant representative for the ionospheric currents.
2 Too many magnetometer stations in any specific area are unavailable, adding to the unreliability of the result.
3 Too many magnetometer stations encounter uncertainties in the baseline derivation, due to equipment drift, long periods without quiet days, or strong variations (see Section 2.8 for explanations of this).
4 None of the above problems; good quality data

In case of a combination of the abovementioned problems, the one associated with a lower number (= more severe) always override those with higher ones.

The definition of 'too many' in the above description is as follows. A condition is true for 'too many' stations if it is true for at least one of the following:

- For 2 or more of the 4 stations under the polar cap: NAL, LYR, HOR, HOP

- For the station on the polar cap boundary: BJN
- For 5 or more of the 16 stations under the auroral oval: NOR, SOR, KEV, TRO, MAS, AND, KIL, IVA, ABK, LEK, MUO, LOZ, KIR, SOD, PEL, DON
- For 4 or more of the 7 stations in the immediate sub-auroral area: RVK, LYC, OUJ, MEK, HAN, DOB, SOL
- For 3 or more of the 4 stations in the lower sub-auroral area: NUR, UPS, KAR, TAR

4.2.5 Functions called

The script calls the following functions:

make_matrix_DF_vector.m

Matlab function for calculating matrices which give the theta- and phi-components of a vector field from the scaling factors of div-free spherical elementary current systems (DF SECS).

make_matrix_DF_magnetic.m

Matlab function for calculating matrices that relate the (ground) magnetic field to the SECS representation.

inv_SVD.m

Matrix inversion using singular value decomposition.

4.3. Online software

Although significant effort in this project was put to the development for a baseline determination routine which works reliably in variable conditions, in some special cases the users may want to use their own baseline information. For such cases a software module for event analysis will be provided.

This module will allow the user to use a period of quiet time as a baseline for the equivalent current calculation (similarly as has been the common procedure for a long time). The user will be asked to select a period of quiet time. The average value of the recordings from this period will be used as the baselines for equivalent current computation. Next, the user can determine a time instant for which the plot of equivalent current map will be created. The software will then calculate the equivalent currents and produce the requested plot.

This software module will be available to be run online in the homepage of the MIRACLE network maintained by FMI. The homepage already now has this kind of service for the 1D equivalent currents and a tool which helps the users to search suitable quiet time periods for baseline computation.

5 Data files

5.1. CEF files

We have discussed CEF production with the Uppsala group, and have decided to produce the following daily CEF files:

- daily CEF for equivalent currents, where the information about the latitude, longitude, as well as northward and eastward equivalent current density is given;
- CEF for daily magnetic baselines for the *X* and *Y* magnetic component for each of 32 stations (where the possibility of expansion to 40 station is given, in case more stations are used in the future).

Also, we provide some CEF files which are each valid for the entire ten-year period:

- a CEF file for the daily median information for X and Y magnetic component for each station;
- a CEF file for quiet days and harmonics for each station,
- a CEF file for the jumps at each magnetometer station.

6 Graphics

6.1. Quick-look plots

Two types of quick-look plots are produced in this project, which will be available in CAA and from which the calculated equivalent current can be read.

The first type of quick-look plots are daily plots of the eastward current interpolated from the 2-dimensional current data along the meridian of 22 degrees. This shows the diurnal development of the east&west electrojet in the ionosphere. The current is shown as colour plots as a function of time and latitude. A line in these plots also indicates the latitude of the magnetic footprint of the CLUSTER C3 satellite, whenever it was less than 100 km from this meridian. An example of these plots is shown in Figure 12.

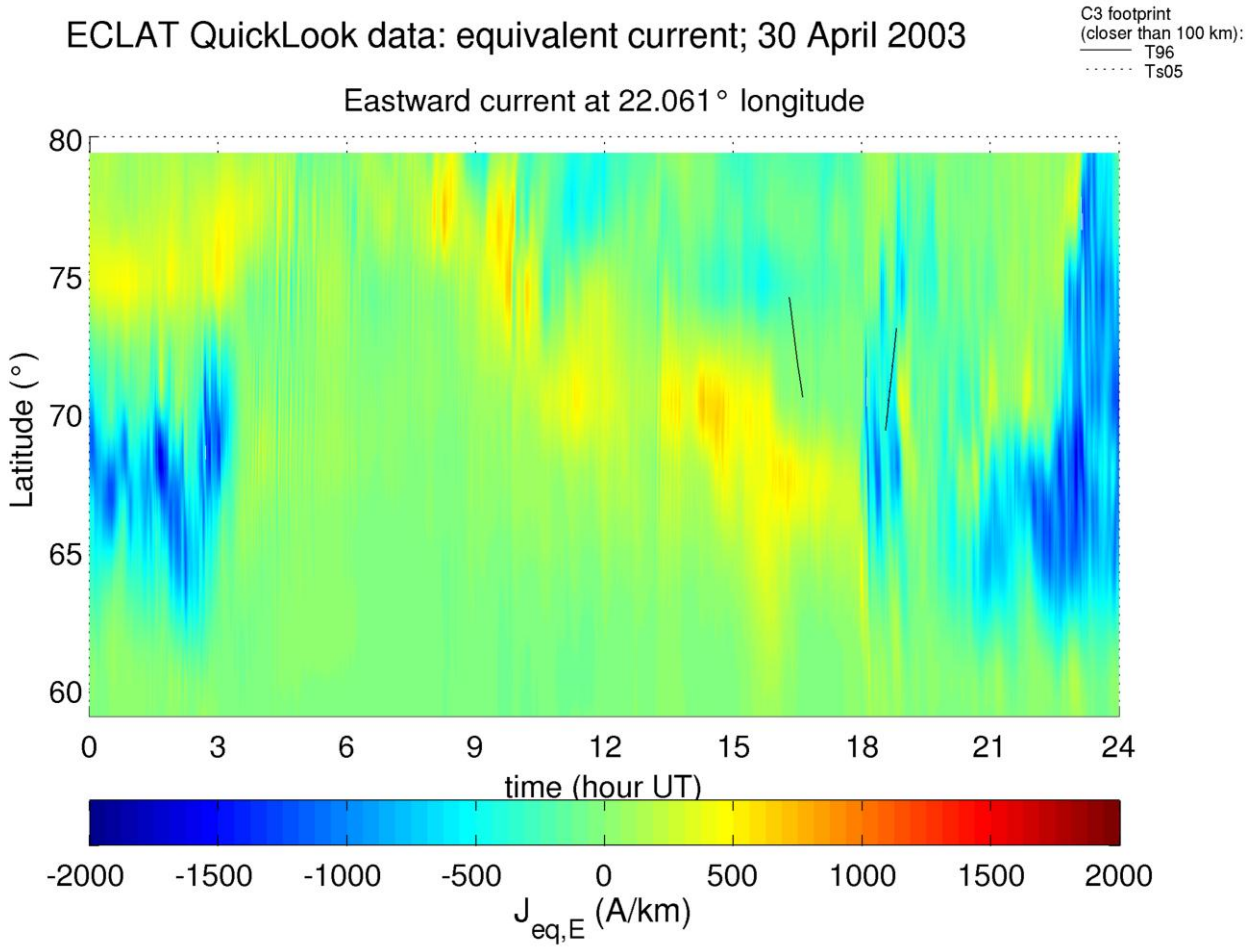

Figure 12. Quick-look plot of the eastward current on 30 April 2003.

The second type of quick-look plots show the 2-D equivalent current for specific moments in time. these are produced with a 1-minute time resolution, with 6 plots combined in one graphic file. The currents are shown as arrows in these plots. The CLUSTER C3 footprint, whenever it is within the range of the graph, is also shown in these plots. An example of these plots is shown in Figure 13.

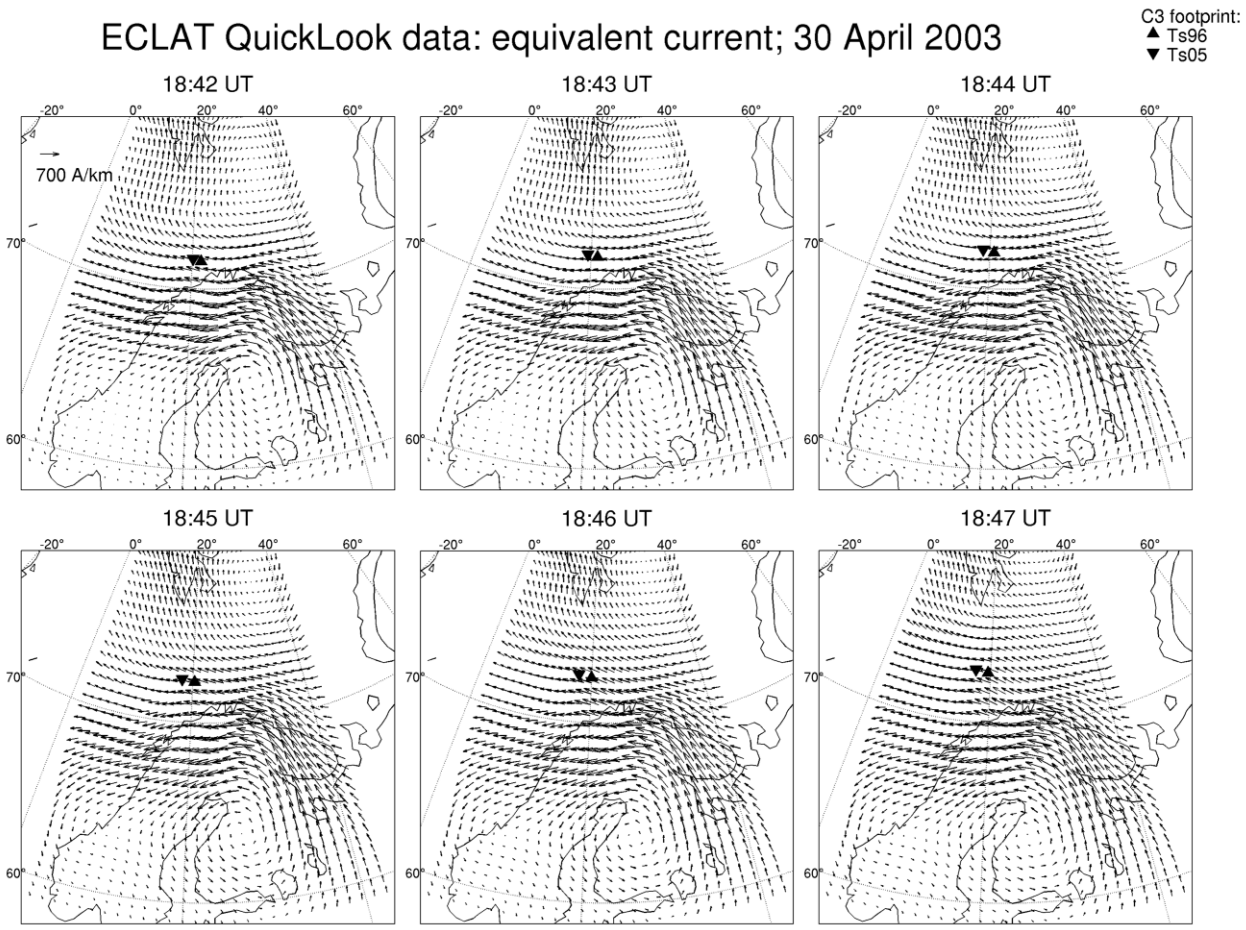

Figure 13. Quick-look plot of the 2-D current on 30 April 2003.

7 References

Amm, O., and A. Viljanen (1999): “Ionospheric disturbance magnetic field continuation from the ground to the ionosphere using spherical elementary current systems”, *Earth Planets Space,* **51**, 431-440.

Bencze, P. (2005): “On the long-term change of ionospheric parameters”, *Journal of Atmospheric and Solar-Terrestrial Physics*, **67**, 1298-1306, doi:10.1016/j.jastp.2005.06.020.

Boteler, D. H., R. J. Pirjola, and H. Nevanlinna (1998): “The effects of geomagnetic disturbances on electrical systems at the earth's surface”, *Adv. Space Res.*, **22**(1), 17-27.

Fukushima, N. (1976): ”Generalized theorem for no ground magnetic effect of vertical currents connected with Pedersen currents in the uniform-conductivity ionosphere, *Rep. Ionos. Space Res. Japan,* **30**, 35-40.

Janzhura, A. S., and O. A. Troshichev (2008): “Determination of the running quiet daily geomagnetic variation”, *Journal of Atmospheric and Solar-Terrestrial Physics*, **70**, 962-972, doi:10.1016/j.jastp.2007.11.004.

Kamide, Y., and W. Baumjohann (1993): *Magnetosphere-Ionosphere Coupling*, *Physics and chemistry in space planetology; vol. 23*, 178 pp. Springer-Verlag, New York.

Laakso, H., C. Perry, S. McCaffrey, D. Herment, A.J. Allen, C.C. Harvey, C.P. Escoubet, C. Gruenberger, M.G.G.T. Taylor, and R. Turner, (2009): Cluster Active Archive: Overview, In “The Cluster Active Archive”, Laakso et al (eds.), *Astrophysics and Space Science Proceedings*, doi:10.1007/978-90-481-3499-1_1.

Pulkkinen, A., O. Amm, A. Viljanen and BEAR Working Group (2003): “Ionospheric equivalent current distributions determined with the method of spherical elementary current systems”, *J. Geophys. Res.*, **108**(A2), 1053, doi: 10.1029/2001JA005085.

Stauning, P. (2011): “Determination of the quiet daily geomagnetic variations for polar regions”, *Journal of Atmospheric and Solar-Terrestrial Physics*, **73**, 2314-2330, doi:10.1016/j.jastp.2011.07.004.

Untiedt, J., and W. Baumjohann (1993): “Studies of polar current systems using the IMS Scandinavian magnetometer array”, *Space Sci. Rev.*, **63**, 245.